

# Selective Targeting of Nanocarriers to Neutrophils and Monocytes

EFSTATHIOS KARATHANASIS,<sup>1</sup> CISSY M. GEIGERMAN,<sup>2</sup> CHARLES A. PARKOS,<sup>2</sup> LESLIE CHAN,<sup>1</sup>  
RAVI V. BELLAMKONDA,<sup>1</sup> and DAVID L. JAYE<sup>2</sup>

<sup>1</sup>Wallace H. Coulter Department of Biomedical Engineering, Georgia Institute of Technology, Atlanta, GA, USA; and  
<sup>2</sup>Department of Pathology and Laboratory Medicine, Emory University School of Medicine, Atlanta, GA, USA

(Received 15 January 2008; accepted 15 April 2009; published online 23 April 2009)

**Abstract**—We previously identified and characterized cell-type selective binding peptides from random peptide phage display libraries. Here, we used one of these peptides (GGP) to target liposomal nanocarriers to leukocyte subsets. To profile the binding selectivity of GGP-coated liposomes to human blood cells, we performed flow cytometric analysis with whole anti-coagulated blood. It is shown that when liposomal nanocarriers present these peptides on their surface, they facilitated cell-type specific targeting of liposomes to neutrophils and monocytes in contrast to nontargeted liposomes. Our data suggest that engineering the appropriate number of targeting peptide ligands on the nanocarrier surface is a factor in cell-binding selectivity, as is dose. Increasing the peptide density on the surface of the liposomes from 250 to 500 molecules resulted in more binding to neutrophils and monocytes. Fluorescence confocal microscopy corroborated the flow cytometry data revealing that liposomes coated with targeting GGP peptides decorated the surface of targeting cells and facilitate cell uptake of payload as evidenced by nuclear localization of tracer. These data suggest that small peptides identified by phage display techniques can be used to target nanocarriers that potentially carry therapeutic or imaging agents to leukocyte subsets. This ability has important implications for diseases where neutrophils and monocytes play a major role such as arthritis, inflammatory bowel disease, chronic obstructive pulmonary disease, and glomerulonephritis.

**Keywords**—Liposomes, Targeting, Phage display, Leukocytes, Inflammation, Nanotechnology.

## INTRODUCTION

Monocytes and neutrophils play key roles in the development and progression of many inflammatory diseases where inflammation becomes detrimental. Such diseases include chronic obstructive pulmonary

disease (COPD), glomerulonephritis, and inflammatory bowel disease (IBD).<sup>11,34,39</sup> For example, elevated levels of neutrophils (reaching about 70% of the total inflammatory cells) and a 5- to 10-fold increase in macrophages are found in sputum and bronchial lavage samples from COPD patients.<sup>42</sup> In many inflammatory diseases, the extent of neutrophilic infiltrates correlates with disease activity and symptoms, and underlies to pathophysiology.<sup>15</sup> To treat and manage the inflammation, potent immunosuppressants such as steroids are commonly employed. Due to the lack of specificity, a range of considerable side-effects may occur including significant psychiatric and systemic metabolic disturbances in many patients.<sup>11</sup> Thus, methods that afford selective targeting of anti-inflammatory agents to the specific cell types of interest, such as neutrophils and monocytes, are needed.

Nanotechnology is playing an important role in providing new types of therapeutic interventions. Systemically administered nanotherapeutics have shown to enhance the therapeutic index of drugs (especially anticancer agents), either by increasing the drug concentration in the site of interest and/or by decreasing the exposure in healthy tissues.<sup>44</sup> Nanoscale delivery systems offer the potential of multifunctional platforms<sup>4,35,37</sup> due to their ability to (i) carry large “payloads” of one or more types of drugs for therapy or contrast agents for imaging or combinations of drugs and contrast agents and (ii) manipulate pharmacokinetics and biodistribution of systemically administered agents. Nanocarriers can theoretically be designed to passively and actively target sites of interest. Passive targeting results from prolonged circulation of nanocarriers allowing for accumulation at sites with abnormal, leaky vasculature such as cancerous and inflamed tissues. This preferential accumulation, termed the enhanced permeation and retention (EPR) effect, occurs due to passive convective transport through leaky endothelium.<sup>8,10,24</sup> Since the convective transport of these particles far

Address correspondence to David L. Jaye, Department of Pathology and Laboratory Medicine, Emory University School of Medicine, EUH, H190, 1364 Clifton Road NE, Atlanta, GA 30322, USA. Electronic mail: ravi@bme.gatech.edu, dljaye@emory.edu

outweighs the diffusive component, they do not generally return to the blood stream, in contrast to small molecules. To further increase targeting affinity and selectivity, nanocarriers can be tagged with targeting molecules (e.g., antibodies) that bind to specific-targeting receptors that are expressed on cells of interest for active targeting.<sup>7,36</sup>

Cell-targeting peptides have been used to develop actively targeted gold and magnetic nanocarriers, including quantum dots, for therapy<sup>2,3,22,27,30,41,43</sup> and imaging.<sup>19–21,31,33</sup> Random peptide phage display libraries provide a potent basis for identification of cell-type selective targeting moieties. Libraries that contain up to  $10^9$  unique oligopeptide sequences in a small volume can afford rapid screening of immense numbers of peptides to identify distinctive cell-surface signatures. However, the use of phage derived cell-targeting peptides with liposomal nanocarriers has not been extensively studied. We previously identified phage bearing peptides with the GPNLTGRW consensus motif and observed that a representative phage, bearing peptide FGPNLTGRW, binds selectively to human neutrophils and monocytes, but not other blood cells.<sup>12,14,26</sup> In this study, we employed the motif-containing synthetic peptide GGPNLTGRW (GGP) which acts as a specific competitive inhibitor of FGP phage binding, and displays neutrophil and monocyte selective binding.<sup>13,26</sup> We fabricated a liposomal nanocarrier coated with the GGP peptide, using doxorubicin as a model payload with detectable fluorescence, and show that the peptide engenders selective targeting of the liposomes to neutrophils and monocytes in a mixture as complex as whole blood.

## MATERIALS AND METHODS

### Materials

Purchased reagents included phospholipid 1,2-dipalmitoyl-*sn*-glycero-3-phosphatidylcholine (DPPC; Genzyme Pharmaceuticals, Cambridge, MA), cholesterol (Sigma, St. Louis, MO), DSPE-PEG2000-COOH (Avanti Polar Lipids, Birmingham, AL), cross-linker *N,N*-dicyclohexylcarbodiimide (DCC; Pierce, Rockford, IL), extra dry DMSO and pyridine (Fisher Scientific, Atlanta, GA), 100 kDa molecular-weight cutoff (MWCO) dialysis tubing (Spectra/Por, Dominguez, CA), doxorubicin (Bedford Laboratories, Bedford, OH). The peptide Ac-GGPNLTGRWGPPVESALAK-NH<sub>2</sub> (GGP peptide) was synthesized by Global Peptide, Inc (Fort Collins, CO) using standard Fmoc chemistry followed by HPLC purification and sequence confirmation by mass spectroscopy.

### Synthesis of Peptide Conjugates

A lipid-PEG-peptide conjugate was synthesized that could later be incorporated into liposomes for targeting. Since the specific binding activity of the GGP peptide is at the amino terminus,<sup>26</sup> carboxyl-terminus was used for conjugate synthesis. The zero length cross-linker DCC was used to couple the carboxyl group of DSPE-PEG-COOH to the peptide primary amine.<sup>6</sup> The C-terminus had been acetylated during synthesis to preclude peptide polymerization. Figure 1 shows the reaction scheme and structure of the final conjugate. Briefly, 10.9 mg (5.6  $\mu$ mol) of GGP peptide were dissolved in 500  $\mu$ L of DMSO. DSPE-PEG(2000)-COOH

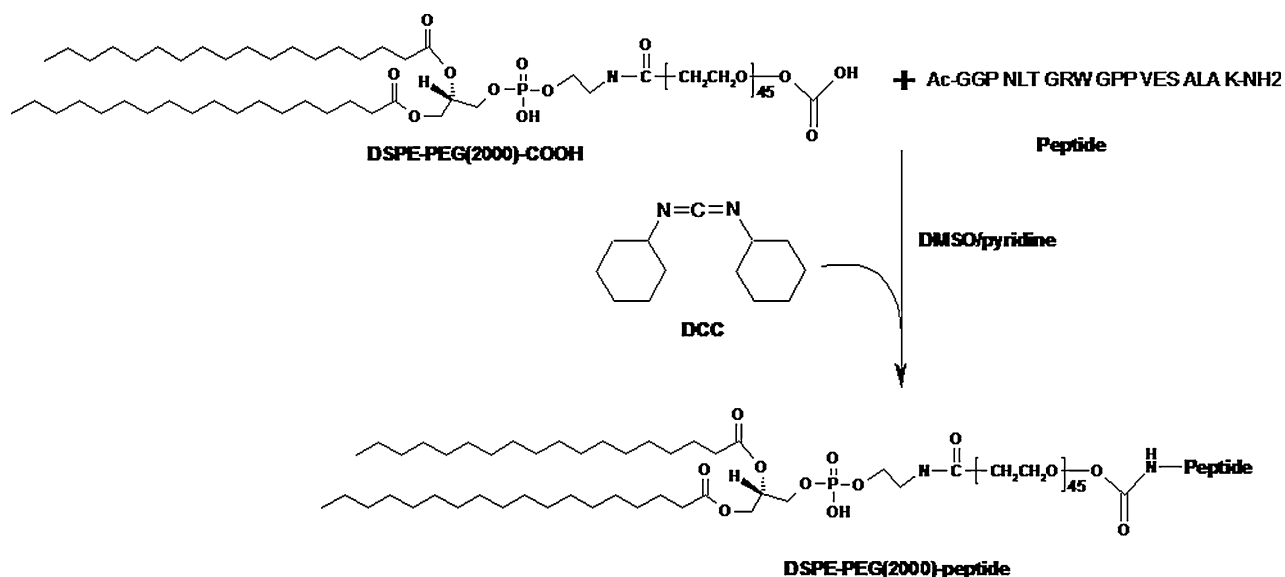


FIGURE 1. Synthetic process of the DSPE-PEG-peptide conjugate.

(10 mg, 3.5  $\mu\text{mol}$ ), DCC (10.8 mg, 52.6  $\mu\text{mol}$ ) and 250  $\mu\text{L}$  of pyridine were added to the reaction which proceeded for 6 h at ambient temperature. Pyridine was removed by rotary evaporation. Conjugate micelles were formed by hydrating the DMSO solution with 5 mL of DI water such that DMSO represented 10% final volume. Unreacted compounds were removed by dialysis (100 kDa MWCO) against 1 L, 50 mM NaCl (2 $\times$ ) and 1 L of DI water (2 $\times$ ) followed by lyophilization. Final peptide content was determined using the DC protein assay (Bio-Rad, Hercules, CA). The final conjugate was characterized by thin layer chromatography (TLC) on pre-coated plates (silica gel 60 F254) and MALDI-TOF mass spectroscopy (Applied Biosystems 4700 proteomics analyzer) to confirm molecular mass, with spectrum obtained in negative ion mode in *a*-cyano-4-hydroxycinnamic acid (CHCA) matrix.

#### *Preparation and Characterization of Liposomes*

Liposomes were prepared by extruding a suspension of dissolved hydrated lipids through Whatman Nucleopore polycarbonate membranes in a Lipex Biomembranes Extruder (Northern Lipids, Vancouver, Canada). A lipid composition of 59.99- $x$  mol% DPPC, 40 mol% cholesterol, and  $x$  mol% DSPE-PEG-peptide conjugate was used.  $\beta$ -DPH, fluorescent phospholipid (Invitrogen, Carlsbad, CA), at 0.01 mol% of the lipid content was used to track phospholipid content. Three liposomal formulations were prepared by varying the number of ligands (peptides) per liposome: (1) nontargeted liposomes where  $x = 0$  (NTL), (2) 250 ligands on the external leaflet per liposome where  $x = 0.06$  (TL-250), and (3) 500 ligands on the external leaflet per liposome where  $x = 0.12$  (TL-500). The lipids were dissolved in ethanol at 60 °C and then hydrated for 2 h with a 400 mM ammonium sulfate solution with ethanol  $\leq 10\%$  of final volume, and 25 mM final lipid concentration. The suspension was passed four times with a 0.2- $\mu\text{m}$  membrane and eight times with a 0.1- $\mu\text{m}$  membrane through the extruder at 60 °C and a pressure of approximately 100 psi. Liposomes were dialyzed (100 kDa MWCO) against phosphate-buffered saline (PBS) to establish an ammonium sulfate gradient. Liposome size was determined by dynamic light scattering (90 Plus Particle Size Analyzer, Brookhaven Instruments, Holtsville, NY). Liposome-coupled peptide was determined using the DC protein assay (Bio-Rad, Hercules, CA) after lysis of liposomes with 20% SDS. The average peptide number per liposome was determined by a ligand-to-phospholipid ratio, assuming 120,000 phospholipid molecules per

liposome where phospholipid content was quantified by DPH fluorescence.

#### *Remote Loading of Doxorubicin into Liposomes*

Doxorubicin (DOX) was selected for determining the targeting efficiency of liposomes because it can be efficiently loaded into liposomes via a pH gradient, and is easily quantifiable as a fluorophor. Liposomes were loaded with DOX by an ammonium sulfate gradient.<sup>1</sup> Briefly, liposomes and 10 mg/mL DOX were mixed at a ratio of 0.2 mg DOX per mg of DPPC in the liposomes. The liposome-DOX suspension was heated at 60 °C for 1 h. Liposomes were cooled immediately on ice and dialyzed (100 kDa MWCO) twice against PBS to remove free DOX. The final DOX concentration after dialysis was determined after liposome lysis with 10% Triton X-100 by UV absorbance at 480 nm.<sup>25</sup>

#### *Flow Cytometry*

Whole blood was obtained from healthy volunteers by standard phlebotomy using an institutionally approved protocol (IRB protocol number at Emory University 630-97). Blood was anti-coagulated with 3.8% sodium citrate. Liposome preparations were added to 200  $\mu\text{L}$  blood for 3 h at 37 °C with gentle rocking. After washing with PBS, 0.5% BSA, red cells underwent hypotonic lysis as described.<sup>13</sup> Cell pellets enriched in white cells were washed and resuspended in 300  $\mu\text{L}$  PBS, 0.5% BSA for flow cytometry. Data acquisition, on a FACSCanto II<sup>TM</sup> cytometer (BD Biosciences, San Jose, CA), and analysis were accomplished using FlowJo, version 7.2 (TreeStar, Ashland, OR). Standard criteria were used for placing gates on granulocytes, monocytes, and lymphocytes based on forward by right angle light scatter.<sup>13</sup> Studies were performed on three donors.

#### *Immunofluorescence Microscopy*

Blood cells were incubated with liposome preparations as for flow cytometry studies. After red cell lysis, white cells were allowed to attach to glass slides for 30 min prior to microscopy as described.<sup>13</sup> Briefly, slides were washed, fixed with 3.7% paraformaldehyde, and nuclei counterstained with topro-3-iodide (Molecular Probes, Carlsbad, CA). Slides were cover slipped for viewing on a Zeiss LSM510 laser scanning confocal microscope coupled to a Zeiss 100 M axiovert and 100 $\times$  Pan-Apochromat oil lense (Zeiss Microimaging, Thornwood, NY). Images were processed using Adobe Photoshop CS3 version 10.0.01.

## RESULTS AND DISCUSSION

## Flow Cytometric Analysis

## Characterization of DSPE-PEG-Peptide Conjugate

The final product characterized by TLC showed no unreacted peptide as evidenced by an absence of ninhydrin staining. Cupric sulfate spray indicated complete consumption of the DSPE-PEG-COOH (disappearance of the parent spot,  $R_f = 0.4$  in  $\text{CHCl}_3$ : $\text{MeOH} = 85:15$ ) into the desired DSPE-PEG-peptide conjugate (appearance of a new spot,  $R_f = 0.51$  in  $\text{CHCl}_3$ : $\text{MeOH} = 85:15$ ). The peptide content of the conjugate was 95% of the theoretical maximum. In addition, MALDI-TOF mass spectroscopy confirmed that the molecular mass of the conjugate had a bell-shaped distribution of 44 Da-spaced lines indicating a singly charged PEG conjugate. The distribution had its mode at 4,724 Da, in good agreement with the theoretical molecular mass (~4779 Da).

## Characterization of Liposomes

All three liposomal formulations, extruded through a 100 nm polycarbonate membrane, exhibited a similar mean intensity-weighted hydrodynamic diameter of 122–128 nm with a polydispersity index of 0.106–0.120. The formation of liposomes with widely distributed diameters when saturated lipid multi-lamellar vesicles are extruded through such membranes has previously been demonstrated by Sood.<sup>38</sup> The final lipid content, measured by tracking the fluorescent phospholipid  $\beta$ -DPH, was found to be ~20 mM which is consistent with the dilutions mandated by the liposome fabrication protocol. DOX loading efficiency was 95–99% resulting in a final encapsulated DOX concentration of 2.7–2.9 mg/mL. Protein assays verified that the TL-250 and TL-500 formulations contained on average approximately 250 and 500 peptide ligands on the external leaflet per liposome, respectively.

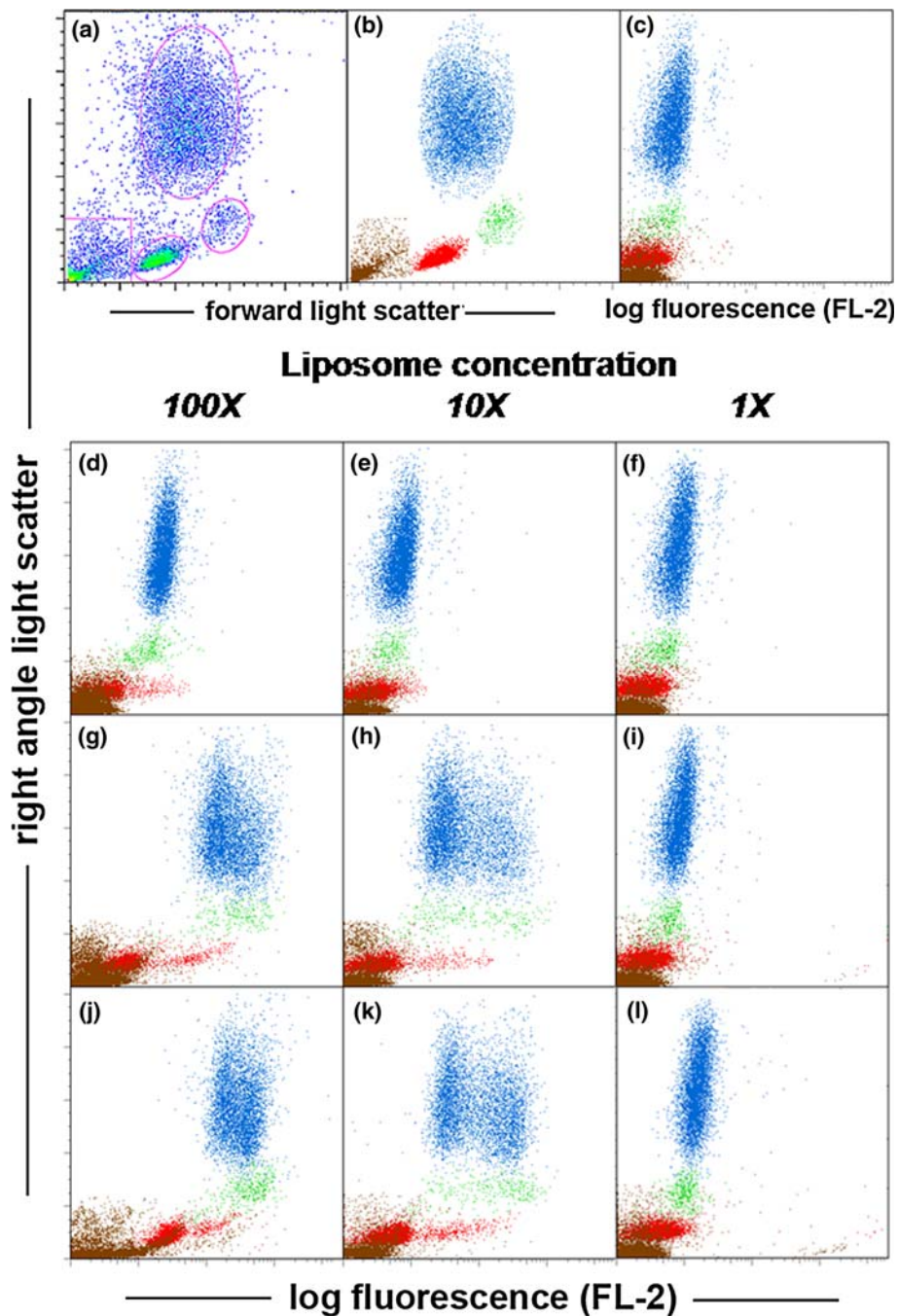
To profile the binding selectivity of GGP-coated liposomes to human blood cells, we performed flow cytometric analysis (FACS). Experiments were performed with whole anti-coagulated blood, including all cells and plasma, from human donors. Blood was incubated at 37 °C with liposome formulations at three concentrations of the across three orders of magnitude (indicated as 1 $\times$ , 10 $\times$ , and 100 $\times$ ). Table 1 summarizes the experimental conditions. Using standard FACS criteria,<sup>13</sup> specific cell populations were gated based on forward by right angle light scatter plots as shown in Fig. 2a. Gated populations are color-coded in Fig. 2b to indicate subpopulations composed of neutrophils (blue), monocytes (green), lymphocytes (red), and residual red cells, platelets, debris and liposomes (brown). Most free residual liposomes were excluded from the plots based on their exceedingly low forward scatter properties.

Figure 2c displays the endogenous baseline fluorescence properties of the gated populations in the absence of liposomes. Results for nontargeted liposomes (NTL) are displayed in the top row, Figs. 2d–2f. As shown, cell associated fluorescence is similar to baseline, suggesting minimal targeting of NTL at the 1 $\times$  and 10 $\times$  doses, though a small shift is seen for monocyte and neutrophil populations at the 100 $\times$  dose. By contrast, selective binding of GGP-coated liposomes, particularly to monocytes and neutrophils is suggested in Figs. 2g–2i, in comparison to NTL at the same concentrations. The cell-type pattern of binding indicates that increasing number of targeting GGP peptides per liposome and increasing liposome concentration correlates with increasing binding. Nonetheless, the binding selectivity decreases at the 100 $\times$  dose for both the TL-500 and TL-250 formulations such that nonspecific shifts occur for the lymphocyte populations. The basis for the bimodal pattern observed for the intermediate dose for

TABLE 1. Summary of the experimental conditions for flow cytometry studies.

Experiment ID	Treatment Type	Liposomes/mL blood	Liposomes added/white blood cell <sup>a</sup>
0 $\times$	No liposomes	0	0
NT (1 $\times$ )	Nontargeted	$1.1 \times 10^{10}$	$2.2 \times 10^3$
NT (10 $\times$ )	Nontargeted	$1.1 \times 10^{11}$	$2.2 \times 10^4$
NT (100 $\times$ )	Nontargeted	$1.1 \times 10^{12}$	$2.2 \times 10^5$
TL-250 (1 $\times$ )	Targeted; coated with 250 GGP	$1.1 \times 10^{10}$	$2.2 \times 10^3$
TL-250 (10 $\times$ )	Targeted; coated with 250 GGP	$1.1 \times 10^{11}$	$2.2 \times 10^4$
TL-250 (100 $\times$ )	Targeted; coated with 250 GGP	$1.1 \times 10^{12}$	$2.2 \times 10^5$
TL-500 (1 $\times$ )	Targeted; coated with 500 GGP	$1.1 \times 10^{10}$	$2.2 \times 10^3$
TL-500 (10 $\times$ )	Targeted; coated with 500 GGP	$1.1 \times 10^{11}$	$2.2 \times 10^4$
TL-500 (100 $\times$ )	Targeted; coated with 500 GGP	$1.1 \times 10^{12}$	$2.2 \times 10^5$

<sup>a</sup>Total white blood cell counts used for the calculation are estimated at 5000/ $\mu\text{L}$  based on a standard reference range of 4000–11,000/ $\mu\text{L}$ .



**FIGURE 2.** Selectivity of peptide nanocarriers binding to leukocyte sub-populations. Liposomes added to acid anti-coagulated whole blood. After RBC lysis, cells underwent FACS. DOX fluorescence detected in FL-2 channel; (a) ungated forward scatter  $\times$  right angle light side scatter plot showing placement of gates for leukocyte subsets; (b) gated subsets shown as neutrophils (*blue*), monocytes (*green*), lymphocytes (*red*), residual red cells, platelets, debris, and liposomes (*brown*); (c) no liposomes. Conditions for which incubations included liposomal preparations were (d) NTL (100 $\times$ ); (e) NTL (10 $\times$ ); (f) NTL (1 $\times$ ); (g) TL-250 (100 $\times$ ); (h) TL-250 (10 $\times$ ); (i) TL-250 (1 $\times$ ); (j) TL-500 (100 $\times$ ); (k) TL-500 (10 $\times$ ); (l) TL-500 (1 $\times$ ).

both formulations (Figs. 2h and 2k) is uncertain. Similar results were obtained for two additional blood donors. When liposomes were incubated with blood at ambient temperature, the FACS profile for both targeting and nontargeting liposomes showed a pattern

similar to that of the nontargeting liposomes in Figs. 2d–2f, suggesting that liposome association with cells is temperature dependent (data not shown). Binding of NTL and targeting formulations to red cells and platelets is minimal for all conditions.

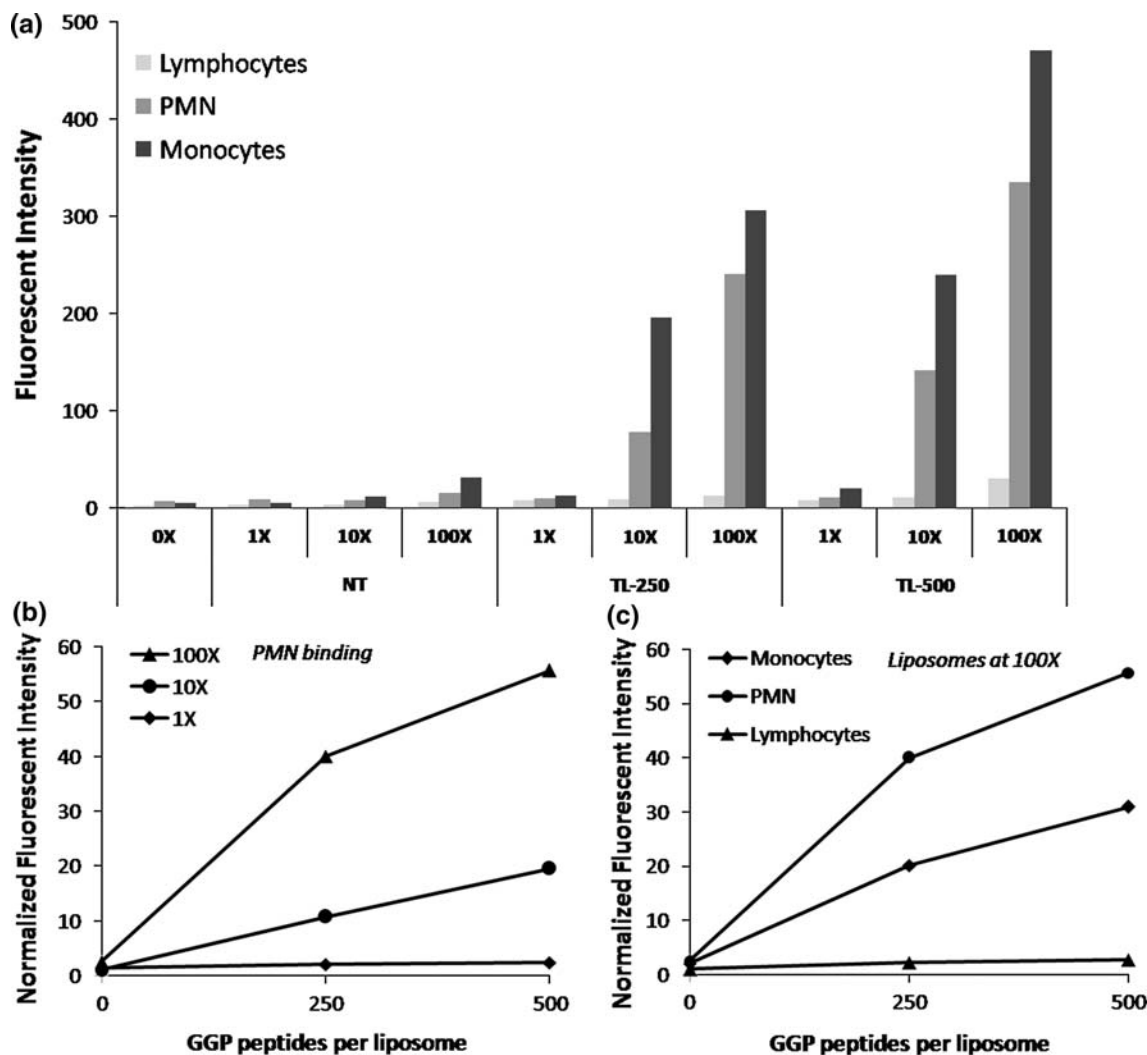


**FIGURE 3.** Liposome dose and peptide dependence of liposome binding. (a) The mean fluorescent intensities (MFI) of gated leukocyte populations are classified based on liposome formulation (NTL, TL-250 and TL-500) and relative binding avidity for leukocyte subsets at the three different concentrations. (b) Relative binding of liposomes to neutrophils (PMN) is displayed as a function of peptide number per liposome and liposome dose by determining normalized MFI where normalized MFI = MFI (cell type, TL-250 or 500)/MFI (cell type, NTL). (c) Normalized MFI are shown suggest relative binding avidities of liposomes to the three major leukocyte subsets at the high liposome concentration (100×) and as a function of peptide number per liposome.

To quantify the FACS binding data, Fig. 3a compares the mean fluorescent intensities (MFIs) of the different liposome formulations as a reflection of relative binding avidities. Nontargeted formulations (NTL) showed minimal binding to all leukocyte subsets in comparison to the control (0×; no liposomes). Binding to neutrophils and monocytes by the GGP-coated liposomes (TL-250) observed at the medium and high liposome concentrations (10× and 100) with greater binding occurring at higher concentrations of liposomes. The low liposome concentration (1×) yielded minimal binding, despite a concentration of approximately  $1 \times 10^{10}$ /mL for all formulations, suggesting a concentration threshold exists for liposomes to bind. Increasing the peptide density on the surface of the

liposomes resulted in more binding to neutrophils and monocytes, comparing TL-500 to TL-250 results. Minimal binding to lymphocytes was suggested at lower liposome concentrations, though some increase was found at the highest concentration tested.

Relative peptide-dependence and selectivities of binding were determined by normalizing MFIs for targeting liposomes to that of the NTL formulation for each cell type. Figure 3b indicates the relative peptide-dependence of the different nanocarrier formulations for neutrophils. For example, binding of the TL-250 and TL-500 formulations is 40 and 55.6 times higher, respectively, than the nontargeted formulation at 100× concentrations. Additionally, the TL-500 formulation at 100× showed a 2.8 times higher relative binding

than at the 10× concentration. These findings suggest a marked increase in binding to the neutrophils mediated by the high valency presentation of peptide on the liposome surface. As displayed in Fig. 3c, the relative binding selectivity for neutrophils is better than for monocytes regardless of the GGP peptide density at 100×, and 10× (not shown), concentrations. Here, the TL-500 formulation showed a relative binding avidity for neutrophils, monocytes, and lymphocytes that was 55.6, 30.9, and 2.7 times higher, respectively, than the NTL formulation. Little relative increase over NTL for lymphocyte binding is noted regardless of peptide density or liposome dose.

The liposomal bilayer is composed primarily of phosphatidylcholine (DPPC). At physiologic pH, the choline carries a positive charge and the phosphate a negative charge yielding a charge-neutral hydrophilic head group. Since phospholipids number approximately 55,000 molecules per liposome, phospholipid contribution to nanocarrier surface charge per area is likely to be much larger compared to that of the peptides which number only about 250 or 500 per liposome. Similar FACS experiments were performed to profile blood cell binding with a nanocarrier coated with a nontargeting control peptide GSTRMGIPA that bears the same net charge as the GGP peptide (at pH 7.0 net charge = 1,  $pI = 11$ ). This control nanocarrier displayed minimal binding to leukocyte subsets (data not shown). This finding is consistent with the hypothesis that the charge of the surface peptide alone does not determine binding selectivity of nanocarriers to neutrophils and monocytes and points to importance of specific amino acid sequence.

#### *Immunofluorescence Microscopy*

Immunofluorescence confocal microscopy was performed to determine the subcellular localization of the DOX payload and test the peptide dependence of targeting. For this study, the NT, TL-250, and TL-500 liposome formulations were incubated with whole

blood as above. Harvested blood cells were allowed to attach to glass slides followed by fixation and nuclear counterstaining to identify nucleated cells. As shown in Fig. 4, NT liposomes (Fig. 4b) display a similar general absence of DOX associated fluorescence, similar to the control background fluorescence in the absence of added liposomes (Fig. 4a). Rare cell surface associated DOX was observed (Fig. 4c, inset) for liposomes coated with random control nontargeting peptide (RPGNGWLGT, average 500/liposome), with same net charge as the GGP peptide at physiologic pH. In contrast, Figs. 4d and 4e show DOX-related fluorescence for both the TL-250 and TL-500 liposome conditions (red) decorating the surface of numerous cells. In addition, many of these cells with neutrophil nuclear features display nuclear reactivity as well with colocalization of the DOX (red) and nuclear counterstains (blue) engendering purple (Figs. 4d and 4e insets). Thus, these data corroborate the flow cytometry data and are consistent with enhanced binding of liposomes coated with targeting GGP peptides. Moreover, they suggest that a portion of the DOX payload is taken up by cells as evidenced by nuclear localization. Of note, even though most drugs have to be taken up by the targeted cells to be effective, internalization of the entire nanocarrier is not required. In fact, targeting nanocarriers can be designed to serve as vehicles for the controlled-release of drugs. Hence, selective targeting of the nanocarriers to the cells of interest can improve targeted drug delivery even in the absence of liposome uptake. For example, we have recently shown that a different cell-targeting nanocarrier can be used as an imaging agent for radiographic detection when loaded with a contrast agent, whether it is taken up or maintains cell-surface association.<sup>16–18</sup>

#### CONCLUSIONS

In this work, we demonstrate the ability of a cell-type specific targeting peptide identified from a

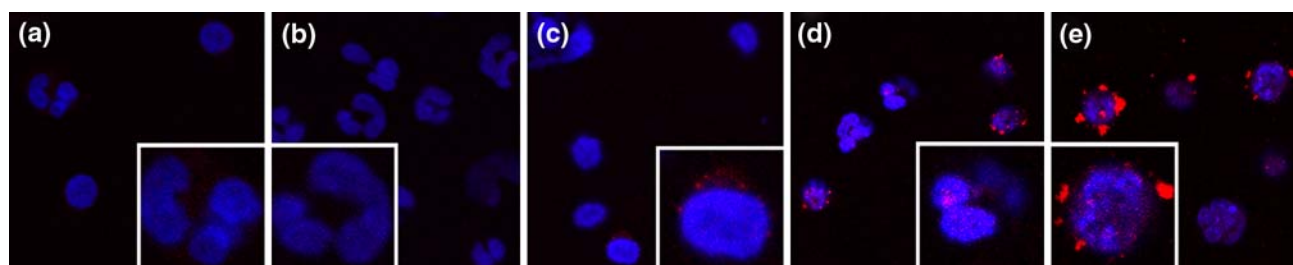


**FIGURE 4.** Cellular localization of peptide nanocarriers and DOX payload. Liposomes added to anti-coagulated whole blood. After red cell lysis, white cells were allowed to attach to glass slides, fixed and cover-slipped for confocal photomicroscopy. Confocal microscopic images were acquired en face of (a) no liposomes; (b) nontargeting liposomes; (c) control peptide liposome; (d) TL-250, and (e) TL-500. Topro-3-iodide counter nuclear stain is shown in blue. DOX fluorescence is indicated in red.

random peptide phage display library,<sup>26</sup> to imbue similar targeting selectivity to liposomal nanocarriers when presented on the nanocarrier surface. For these proof-of-principle studies, we have used a well-characterized peptide, GGP, that targets leukocyte subsets, specifically neutrophils and monocytes.<sup>12,13,26</sup> There are, in fact, inflammatory diseases including IBD, various forms of glomerulonephritis, and asthma for which both neutrophils and monocytes play roles in pathobiology and knocking out both may be clinically useful<sup>5,23,40</sup> using the nanocarrier we studied here. Nonetheless, selection of peptides for nanocarriers that could target either neutrophils or monocytes individually is feasible<sup>26</sup> and represents a complementary approach for specific cell-type targeting of cells, such as monocytes and neutrophils that demonstrate distinct and overlapping roles in inflammation.

While these studies represent *in vitro* analyses with whole blood, we predict that systemically administered nanoscale agents would readily access sites of inflammation as they generally show enhanced vascular permeability. Angiogenesis, as well, has been well-documented at sites of chronic inflammation resulting in new and remodeled blood microvessels with increased permeability.<sup>28,29,32</sup> Nanocarriers can selectively extravasate and accumulate at sites with compromised vasculature via the EPR effect.<sup>9,24</sup> Moreover, local nanocarrier application or injection into specific anatomic compartments affected by inflammation represents alternative delivery routes.

Not surprisingly, our data suggest that engineering the appropriate number of targeting peptide ligands on the nanocarrier surface is a factor in cell-binding selectivity, as is dose. Here, liposomes coated with this peptide were targeted to neutrophils and monocytes when exposed to the immense cellular and protein complexity of whole human blood, including red cells with a 1000-fold greater concentration than neutrophils and monocytes. Such a nanocarrier could potentially serve as a delivery system of anti-inflammatory drugs to increase their therapeutic index and of contrast agents to allow detection and characterization of inflammatory diseases. We envision, therefore, that such selective targeting of specific leukocytes can offer nanoscale delivery platforms for diagnosis and treatment of inflammatory diseases.

#### ACKNOWLEDGMENTS

This work was supported in part by grants from the NIH DK60647 and DK064399 (D.L.J.) and the Georgia Cancer Coalition (R.V.B.).

#### REFERENCES

- <sup>1</sup>Bolotin, E., R. Cohen, L. Bar, N. Emanuel, S. Ninio, D. Lasic, and Y. Barenholz. Ammonium sulfate gradients for efficient and stable remote loading of amphipathic weak bases into liposomes and ligandoliposomes. *J. Liposome Res.* 4:455–479, 1994. doi:10.3109/08982109409037057.
- <sup>2</sup>Derfus, A. M., A. A. Chen, D. H. Min, E. Ruoslahti, and S. N. Bhatia. Targeted quantum dot conjugates for siRNA delivery. *Bioconjugate Chem.* 18(5):1391–1396, 2007. doi:10.1021/bc060367e.
- <sup>3</sup>Farokhzad, O. C., S. Jon, A. Khademhosseini, T. N. Tran, D. A. Lavan, and R. Langer. Nanoparticle-aptamer bioconjugates: a new approach for targeting prostate cancer cells. *Cancer Res.* 64(21):7668–7672, 2004. doi:10.1158/0008-5472.CAN-04-2550.
- <sup>4</sup>Ferrari, M. Cancer nanotechnology: opportunities and challenges. *Nat. Rev. Cancer* 5(3):161–171, 2005. doi:10.1038/nrc1566.
- <sup>5</sup>Hanauer, S. B. Inflammatory bowel disease: epidemiology, pathogenesis, and therapeutic opportunities. *Inflamm. Bowel Dis.* 12(Suppl 1):S3–9, 2006. doi:10.1097/01.MIB.000195385.19268.68.
- <sup>6</sup>Hermanson, G. *Bioconjugate Techniques*. New York: Academic Press, 1996.
- <sup>7</sup>Hong, S., P. R. Leroueil, I. J. Majoros, B. G. Orr, J. R. Baker, Jr., and M. M. Banaszak Holl. The binding avidity of a nanoparticle-based multivalent targeted drug delivery platform. *Chem. Biol.* 14(1):107–115, 2007. doi:10.1016/j.chembiol.2006.11.015.
- <sup>8</sup>Jain, R. K. Barriers to drug delivery in solid tumors. *Sci. Am.* 271(1):58–65, 1994.
- <sup>9</sup>Jain, R. K. Transport of molecules, particles, and cells in solid tumors. *Annu. Rev. Biomed. Eng.* 1:241–263, 1999. doi:10.1146/annurev.bioeng.1.1.241.
- <sup>10</sup>Jain, R. K. Delivery of molecular and cellular medicine to solid tumors. *Adv. Drug Deliv. Rev.* 46(1–3):149–168, 2001. doi:10.1016/S0169-409X(00)00131-9.
- <sup>11</sup>Javaid, B., and R. J. Quigg. Treatment of glomerulonephritis: will we ever have options other than steroids and cytotoxics? *Kidney Int.* 67(5):1692–1703, 2005. doi:10.1111/j.1523-1755.2005.00266.x.
- <sup>12</sup>Jaye, D. L., H. A. Edens, L. Mazzucchelli, and C. A. Parkos. Novel G protein-coupled responses in leukocytes elicited by a chemotactic bacteriophage displaying a cell type-selective binding peptide. *J. Immunol.* 166(12):7250–7259, 2001.
- <sup>13</sup>Jaye, D. L., C. M. Geigerman, R. E. Fuller, A. Akyildiz, and C. A. Parkos. Direct fluorochrome labeling of phage display library clones for studying binding specificities: applications in flow cytometry and fluorescence microscopy. *J. Immunol. Methods* 295(1–2):119–127, 2004. doi:10.1016/j.jim.2004.09.011.
- <sup>14</sup>Jaye, D. L., F. S. Nolte, L. Mazzucchelli, C. Geigerman, A. Akyildiz, and C. A. Parkos. Use of real-time polymerase chain reaction to identify cell- and tissue-type-selective peptides by phage display. *Am. J. Pathol.* 162(5):1419–1429, 2003.
- <sup>15</sup>Jaye, D. L., and C. A. Parkos. Neutrophil migration across intestinal epithelium. *Ann. NY Acad. Sci.* 915:151–161, 2000.
- <sup>16</sup>Karathanasis, E., L. Chan, S. R. Balusu, C. J. D’Orsi, A. V. Annapragada, I. Sechopoulos, and R. V. Bellamkonda. Multifunctional nanocarriers for mammographic quantification of tumor dosing and prognosis of breast cancer

- therapy. *Biomaterials* 29(36):4815–4822, 2008. doi:[10.1016/j.biomaterials.2008.08.036](https://doi.org/10.1016/j.biomaterials.2008.08.036).
- <sup>17</sup>Karathanasis, E., J. Park, A. Agarwal, V. Patel, F. Zhao, A. V. Annapragada, X. Hu, R. V. Bellamkonda. MRI mediated, non-invasive tracking of intratumoral distribution of nanocarriers in rat glioma. *Nanotechnology* 19:315101 (315109), 2008.
- <sup>18</sup>Karathanasis, E., S. Suryanarayanan, S. R. Balusu, K. McNeeley, I. Sechopoulos, A. Karellas, A. V. Annapragada, and R. V. Bellamkonda. Imaging nanoprobe for prediction of outcome of nanoparticle chemotherapy by using mammography. *Radiology* 250(2): 398–406, 2009. doi:[10.1148/radiol.2502080801](https://doi.org/10.1148/radiol.2502080801).
- <sup>19</sup>Kelly, K. A., J. R. Allport, A. Tsourkas, V. R. Shinde-Patil, L. Josephson, and R. Weissleder. Detection of vascular adhesion molecule-1 expression using a novel multimodal nanoparticle. *Circulat. Res.* 96(3):327–336, 2005. doi:[10.1161/01.RES.0000155722.17881.dd](https://doi.org/10.1161/01.RES.0000155722.17881.dd).
- <sup>20</sup>Kelly, K. A., P. A. Clemons, A. M. Yu, and R. Weissleder. High-throughput identification of phage-derived imaging agents. *Mol. Imaging* 5(1):24–30, 2006.
- <sup>21</sup>Kelly, K. A., M. Nahrendorf, A. M. Yu, F. Reynolds, and R. Weissleder. In vivo phage display selection yields atherosclerotic plaque targeted peptides for imaging. *Mol. Imaging Biol.* 8(4):201–207, 2006. doi:[10.1007/s11307-006-0043-6](https://doi.org/10.1007/s11307-006-0043-6).
- <sup>22</sup>Kim, J. H., J. S. Kim, H. Choi, S. M. Lee, B. H. Jun, K. N. Yu, E. Kuk, Y. K. Kim, D. H. Jeong, M. H. Cho, and Y. S. Lee. Nanoparticle probes with surface enhanced Raman spectroscopic tags for cellular cancer targeting. *Anal. Chem.* 78(19):6967–6973, 2006. doi:[10.1021/ac0607663](https://doi.org/10.1021/ac0607663).
- <sup>23</sup>Kitching, A. R., S. R. Holdsworth, and M. J. Hickey. Targeting leukocytes in immune glomerular diseases. *Curr. Med. Chem.* 15(5):448–458, 2008. doi:[10.2174/092986708783503230](https://doi.org/10.2174/092986708783503230).
- <sup>24</sup>Maeda, H., J. Wu, T. Sawa, Y. Matsumura, and K. Hori. Tumor vascular permeability and the EPR effect in macromolecular therapeutics: a review. *J. Control Release* 65(1–2): 271–284, 2000. doi:[10.1016/S0168-3659\(99\)00248-5](https://doi.org/10.1016/S0168-3659(99)00248-5).
- <sup>25</sup>Mayer, L. D., M. B. Bally, M. J. Hope, and P. R. Cullis. Uptake of antineoplastic agents into large unilamellar vesicles in response to a membrane potential. *Biochim. Biophys. Acta* 816(2):294–302, 1985. doi:[10.1016/0005-2736\(85\)90497-3](https://doi.org/10.1016/0005-2736(85)90497-3).
- <sup>26</sup>Mazzucchelli, L., J. B. Burritt, A. J. Jesaitis, A. Nusrat, T. W. Liang, A. T. Gewirtz, F. J. Schnell, and C. A. Parkos. Cell-specific peptide binding by human neutrophils. *Blood* 93(5):1738–1748, 1999.
- <sup>27</sup>McCarthy, J. R., K. A. Kelly, E. Y. Sun, and R. Weissleder. Targeted delivery of multifunctional magnetic nanoparticles. *Nanomedicine (London, England)* 2(2):153–167, 2007.
- <sup>28</sup>McDonald, D. M. Angiogenesis and remodeling of airway vasculature in chronic inflammation. *Am. J. Respir. Crit. Care Med.* 164(10 Pt 2):S39–45, 2001.
- <sup>29</sup>McDonald, D. M., G. Thurston, and P. Baluk. Endothelial gaps as sites for plasma leakage in inflammation. *Microcirculation* 6(1):7–22, 1999. doi:[10.1080/713773924](https://doi.org/10.1080/713773924).
- <sup>30</sup>McGuire, M. J., K. F. Sykes, K. N. Samli, L. Timares, M. A. Barry, K. Stemke-Hale, F. Tagliaferri, M. Logan, K. Jansa, A. Takashima, K. C. Brown, and S. A. Johnston. A library-selected, Langerhans cell-targeting peptide enhances an immune response. *DNA Cell Biol.* 23(11):742–752, 2004. doi:[10.1089/dna.2004.23.742](https://doi.org/10.1089/dna.2004.23.742).
- <sup>31</sup>Meng, X. X., J. Q. Wan, M. Jing, S. G. Zhao, W. Cai, and E. Z. Liu. Specific targeting of gliomas with multifunctional superparamagnetic iron oxide nanoparticle optical and magnetic resonance imaging contrast agents. *Acta Pharmacol. Sinica* 28(12):2019–2026, 2007. doi:[10.1111/j.1745-7254.2007.00661.x](https://doi.org/10.1111/j.1745-7254.2007.00661.x).
- <sup>32</sup>Nagy, J. A., L. Benjamin, H. Zeng, A. M. Dvorak, and H. F. Dvorak. Vascular permeability, vascular hyperpermeability and angiogenesis. *Angiogenesis* 11(2):109–119, 2008. doi:[10.1007/s10456-008-9099-z](https://doi.org/10.1007/s10456-008-9099-z).
- <sup>33</sup>Nahrendorf, M., F. A. Jaffer, K. A. Kelly, D. E. Sosnovik, E. Aikawa, P. Libby, and R. Weissleder. Noninvasive vascular cell adhesion molecule-1 imaging identifies inflammatory activation of cells in atherosclerosis. *Circulation* 114(14):1504–1511, 2006. doi:[10.1161/CIRCULATIONAHA.106.646380](https://doi.org/10.1161/CIRCULATIONAHA.106.646380).
- <sup>34</sup>Pillai, D. K., and S. G. Matts. Chronic inflammatory bowel disease—a review. *Br. J. Clin. Pract.* 37(5):165–172, 1983.
- <sup>35</sup>Pope-Harman, A., M. M. Cheng, F. Robertson, J. Sakamoto, and M. Ferrari. Biomedical nanotechnology for cancer. *Med. Clin. North Am.* 91(5):899–927, 2007. doi:[10.1016/j.mcna.2007.05.008](https://doi.org/10.1016/j.mcna.2007.05.008).
- <sup>36</sup>Saul, J. M., A. V. Annapragada, and R. V. Bellamkonda. A dual-ligand approach for enhancing targeting selectivity of therapeutic nanocarriers. *J. Control Release* 114(3):277–287, 2006. doi:[10.1016/j.jconrel.2006.05.028](https://doi.org/10.1016/j.jconrel.2006.05.028).
- <sup>37</sup>Service, R. F. Materials and biology. Nanotechnology takes aim at cancer. *Science* 310(5751):1132–1134, 2005. doi:[10.1126/science.310.5751.1132](https://doi.org/10.1126/science.310.5751.1132).
- <sup>38</sup>Sood, S. Characterization of liposome manufacturing using extrusion. Master's thesis, San Jose State University, 1999.
- <sup>39</sup>Tetley, T. D. Inflammatory cells and chronic obstructive pulmonary disease. *Curr. Drug Targets Inflamm. Allergy* 4(6):607–618, 2005. doi:[10.2174/156801005774912824](https://doi.org/10.2174/156801005774912824).
- <sup>40</sup>Tillie-Leblond, I., P. Gosset, and A. B. Tonnel. Inflammatory events in severe acute asthma. *Allergy* 60(1):23–29, 2005. doi:[10.1111/j.1398-9995.2005.00632.x](https://doi.org/10.1111/j.1398-9995.2005.00632.x).
- <sup>41</sup>Tkachenko, A. G., H. Xie, D. Coleman, W. Glomm, J. Ryan, M. F. Anderson, S. Franzen, and D. L. Feldheim. Multifunctional gold nanoparticle-peptide complexes for nuclear targeting. *J. Am. Chem. Soc.* 125(16):4700–4701, 2003. doi:[10.1021/ja0296935](https://doi.org/10.1021/ja0296935).
- <sup>42</sup>Vlahos, R., S. Bozinovski, J. A. Hamilton, and G. P. Anderson. Therapeutic potential of treating chronic obstructive pulmonary disease (COPD) by neutralising granulocyte macrophage-colony stimulating factor (GM-CSF). *Pharmacol. Ther.* 112(1):106–115, 2006. doi:[10.1016/j.pharmthera.2006.03.007](https://doi.org/10.1016/j.pharmthera.2006.03.007).
- <sup>43</sup>Xie, J., Z. Shen, K. C. Li, and N. Danthi. Tumor angiogenic endothelial cell targeting by a novel integrin-targeted nanoparticle. *Int. J. Nanomed.* 2(3):479–485, 2007.
- <sup>44</sup>Yezhelyev, M. V., X. Gao, Y. Xing, A. Al-Hajj, S. Nie, and R. M. O'Regan. Emerging use of nanoparticles in diagnosis and treatment of breast cancer. *Lancet Oncol.* 7(8):657–667, 2006. doi:[10.1016/S1470-2045\(06\)70793-8](https://doi.org/10.1016/S1470-2045(06)70793-8).